THE ASTROPHYSICAL JOURNAL, 426:204–214, 1994 May 1

MOMENTUM TRANSFER BY ASTROPHYSICAL JETS

LAWRENCE CHERNIN[1] AND COLIN MASSON
Center for Astrophysics, MS 78, 60 Garden Street, Cambridge, MA 02138
E-mail: chernin@ucbast.berkeley.edu; masson@cfa.harvard.edu
ELISABETE M. GOUVEIA DAL PINO
Universidade de São Paulo, Instituto Astronômico e Geofísico Av. Miguel Stéfano, 4200, São Paulo, SP 04301-904, Brazil
AND
WILLY BENZ
University of Arizona, Steward Observatory and Lunar and Planetary Laboratory, Tucson, AZ 85721
Received 1993 June 14; accepted 1993 November 4

ABSTRACT

We have used three dimensional smoothed particle hydrodynamical simulations to study the basic physical properties of the outflow that is created by a protostellar jet in a dense molecular cloud. The dynamics of the jet/cloud interaction is strongly affected by the cooling in the shocked gas behind the bow shock at the head of the jet. We show that this cooling is very rapid, with the cooling distance of the gas much less than the jet radius. Thus, although ambient gas is initially driven away from the jet axis by the high thermal pressure of the post-shock gas, rapid cooling reduces the pressure and the outflow subsequently evolves in a momentum-conserving snowplow fashion. The velocity of the ambient gas is high in the vicinity of the jet head, but decreases rapidly as more material is swept up. Thus, this type of outflow produces extremely high-velocity clumps of post-shock gas which resemble the features seen in outflows.

We have investigated the transfer of momentum from the jet to the ambient medium as a function of the jet parameters. We show that a low Mach number (≤ 6) jet slows down rapidly because it entrains ambient material along its sides. On the other hand, the beam of a high Mach number jet is separated from the ambient gas by a low-density cocoon of post-shock gas, and this jet transfers momentum to the ambient medium principally at the bow shock. In high Mach number jets, as those from young stellar objects, the dominant interaction is therefore at the bow shock at the head of the jet.

Subject headings: hydrodynamics — ISM: jets and outflows — shock waves — stars: mass loss — stars: pre–main-sequence

1. INTRODUCTION

Although over 150 molecular outflows from protostars have been discovered (e.g., Fukui 1989) there is yet to be a consensus on how these flows are driven. These molecular outflows are often associated with Herbig-Haro (HH) objects and highly collimated jets (see Mundt, Brugel, & Bührke 1987, hereafter MBB) with velocities of 100–400 km s^{-1}. On the other hand, most molecular outflows are poorly collimated and have much lower velocities (<20 km s^{-1}). These phenomena may be dynamically related with the jets driving the molecular outflows and producing HH objects where the jets strongly interact with the ambient gas. Apparent discrepancies between the momentum flux in the optically visible component of jets and that in the molecular flows (e.g., MBB) has led to suggestions that the molecular outflows are driven by winds separate from the optically visible jets, but recent evidence that these jets can carry momentum fluxes of 10^{-5} $M_\odot$ km s^{-1} yr^{-1} and that outflows have ages greater than 10^5 yr (Parker, Padman, & Scott 1991), have largely removed the momentum discrepancy (Padman & Richer 1993; Masson & Chernin 1993, hereafter MC). Several authors have begun to explore various models of molecular outflows driven solely by collimated jets (MC; Raga et al. 1993, hereafter RCCRT; Raga & Cabrit 1992, hereafter RC). In this paper we investigate the details of the transfer of momentum from a jet to a quiescent medium with the aid of numerical simulations.

De Young (1986) studied the interaction between a jet and a quiescent medium through numerical simulations and distinguished between two basic processes. The first process is called "prompt entrainment," and is the transfer of momentum through the leading bow shock. The second process is called "steady-state entrainment" and refers to ambient gas that is entrained along the sides of the jet. This type of entrainment is the result of turbulent mixing through Kelvin-Helmholtz instabilities at the velocity shear between the jet and the ambient gas. In the present paper, we distinguish between *entrained* material, which we define as the ambient gas that has been incorporated into the boundary layer and is moving at close to the jet velocity, and *swept-up* material, which we define as the ambient gas that is driven by the jet but may be moving at much lower velocities than the jet. A jet can entrain only a limited amount of material before being disrupted (see De Young 1993). On the other hand, it can sweep up a large quantity of material through the bow shock with very little entrainment. Since we are concerned with the properties of molecular outflows at relatively low velocity, we emphasize the properties of the swept-up material.

If turbulent entrainment along the beam is the dominant process, then jets should decrease in average velocity along their length as they transfer momentum to the entrained material, until the jets eventually become subsonic and the surrounding flow becomes fully turbulent (see Figs. 168 and

[1] Postal address: Department of Astronomy, University of California, Berkeley, CA 94720.

275 of Van Dyke 1982, p. 98; De Young 1993; Stahler 1993). This effect is seen in Figure 4 of De Young (1986), where the jet velocity is plotted as a function of distance along the axis. In the cases he studied, the jet velocity, and hence momentum, could be approximated as an exponential with a scale length which increased more rapidly than the Mach number of the jet. For the Mach 2 jet studied by De Young (1986), the scale length was 15 beam radii, and the jet became subsonic at only 10 beam radii from the origin, while the scale length for the $M = 10$ jet was 168 beam radii. If these results are also applicable to protostellar jets with, for example, Mach numbers of 10–40 and radii 200–2000 AU, the jets are expected to travel a distance of a typical outflow lobe (0.1–0.3 pc) without losing much of their energy (see Cantó & Raga 1990), and the dominant transfer of momentum should occur by the prompt mechanism. This agrees with the observation that jets survive long enough to produce bow shocks which are often seen at the ends of molecular outflows (see Reipurth 1991; Chernin & Masson 1991).

RCCRT modeled a type of turbulent entrainment in which internal bow shocks eject jet material sideways, thereby coupling energy and momentum into a turbulent boundary layer. Lizano et al. (1988) and Stahler (1993) have also suggested that molecular outflows are produced through turbulent mixing. On the other hand, the MC and RC models are based solely on momentum transfer by bow shocks. MC focused on the properties of momentum transfer by a bow shock, and showed how this could account for many of the observed properties of molecular outflows, especially of the extremely high-velocity material, which was identified with the material close to the bow shock. In this model, high thermal pressure at the head of the jet initially drives the ambient gas sideways forming a shroud, but then as the shocked gas rapidly cools, the outflow evolves in a momentum-conserving snowplow fashion. This model provides a good account of the extremely high-velocity (EHV) features, but produces outflows which are too young and too narrow. A more complete model should include aspects of the MC model and long term average characteristics like those considered by RC and RCCRT.

Several authors have used numerical hydrodynamical simulations to study the complex interaction between jets and quiescent media. Simulations of radiative bow shocks have been performed by Blondin, Königl, & Fryxell (1989), Blondin, Fryxell, & Königl (1990, hereafter BFK), Raga (1988), Tenorio-Tagle, Canto, & Rózyczka (1988), Gouveia Dal Pino & Benz (1993, hereafter GDPB) in order to study the features of the bow shocks and the connection with Herbig-Haro objects. Herbig-Haro objects are usually observed where a jet produces a high-velocity, nearly adiabatic bow shock as the jet runs into low density material ($n_{\rm jet} > n_{\rm amb}$). These conditions are usually found at the edges of molecular clouds, or in cavities which may have been partially cleared out by the initial passage of the jet. The previous simulations were therefore made for these low-density conditions ($n_{\rm ambient} < 100$ cm^{-3}), and may not apply directly to the impact of a jet on molecular material in a dense cloud.

To study the dynamics of the transfer of momentum from jets to ambient clouds, we have performed simulations of a jet/cloud interaction with strong cooling using a smoothed particle hydrodynamics (sph) code. The three-dimensional sph code used here is adapted from that used by GDPB. We chose to use a three-dimensional code rather than a high-resolution two-dimensional code in order to retain sensitivity to three-dimensional instabilities, which may be important in the development of the working surface and the outflow. For example, the three-dimensional simulations performed by GDPB showed significant differences with the previous two-dimensional axisymmetric simulations (see BFK; Raga 1988; Tenorio-Tagle et al. 1989).

In § 2 of this paper we outline the numerical method and its limitations, in § 3 we discuss and compare the interactions of the ambient gas with jets of different density and velocity. In § 4 we compare the numerical results with models and discuss the general properties of jet/cloud interactions such as the nature of the shocks. In § 5 we compare our model with the recent millimeter and submillimeter observations of outflows, in particular the extremely high-velocity CO features.

2. NUMERICAL METHOD

We performed fully three-dimensional simulations of radiatively cooling jets using a modified version of the Cartesian smoothed particle hydrodynamics code described in Benz (1990, 1991). Following is a short summary of the key features of the sph technique that are relevant to this work, but for a more detailed discussion see Benz (1990, 1991). Each mass element, or sph particle, is characterized with a position in phase-space ($\boldsymbol{r}$, $\boldsymbol{v}$), mass and specific internal energy, u. The motion of the individual sph particles is easily followed in this scheme and it is therefore trivial to distinguish between particles in the jet and those in the ambient medium. The particles are smoothed out in space with a spherically symmetric kernel function of width h with initial values of 0.4 and 0.2 jet radii for the ambient particles and jet particles, respectively. The initial and boundary conditions are the same as described in GDPB. All distances are normalized to the jet radius, $r_{\rm jet} = 2 \times 10^{16}$ cm. The size of the grid is $-6r_{\rm jet} < x, y < 6r_{\rm jet}$ and $0 < z < 24r_{\rm jet}$ with the jet injected at $z = 0$. About 60,000 sph particles are used in each run, with typical runs taking 1–2 weeks of CPU time on a SPARCstation 2.

Radiative cooling is calculated using a local, time-independent cooling function (Katz 1989). The cooling length, $d_{\rm cool}$, for gas cooling from 10^6 to 10^4 K, calculated using the parameterization given in BFK, is found to be consistent with the parameterization given in Hartigan, Raymond, & Hartmann (1987). Under typical conditions (see below), we find that the bow shock is strongly radiative, $d_{\rm cool} \ll r_j$, and the jet shock is weakly radiative ($d_{\rm cool} \sim r_j$). Thus the subsequent evolution of the ambient gas near the working surface can only be driven by thermal pressure within one jet radius of the jet shock.

For simplicity, the gas is taken to be fully ionized. Shocks at velocities greater than 60 km s^{-1} in a molecular medium use up a negligible fraction of the incident bulk kinetic energy in dissociating the gas, but a substantial fraction of the energy then goes into collisional ionization of the atomic gas (e.g., McKee & Hollenbach 1987; Neufeld & Dalgarno 1989a). Thus our simulations overestimate the temperature of the immediate post-shock gas. Under realistic conditions, the magnetic field would limit the compression of the post-shock gas (Hollenbach & McKee 1979). We also did not include radiative cooling below $T = 7000$ K, when the assumption of an ionized flow breaks down, and radiative cooling is mainly due to molecular formation and molecular lines. The lower limit of 7000 K is not as unrealistic as might appear, as magnetic fields probably provide the dominant form of pressure in the compressed shocked gas at this temperature (Hollenbach & McKee 1979). The dynamics in real molecular clouds are determined by

Alfvén speeds, rather than sound speeds. For example, the observed typical CO line widths of 1–2 km s^{-1} in molecular clouds represents an Alfvén speed rather than a thermal sound speed since these velocities would correspond to unrealistically high gas temperatures of thousands of degrees. Therefore the lack of cooling below 7000 K in our simulations may be partially offset by our neglect of magnetic fields.

There are two other major limitations of sph simulations. Properties of the low-density regions, or cocoons, that may develop between the swept-up gas and the jet beam are poorly sampled because they do not contain as many sph particles as the denser regions. (However, not having to calculate properties of "empty" regions is one of the advantages of sph codes over fixed grid based codes). This becomes a problem only if pressure in the cocoon is large enough to affect the dynamics of the dense shroud (i.e., dynamically significant), but we later show that this is not the case. Secondly, turbulent effects, which exist in these flows (since the Reynolds number, Re, is vey high) are very difficult to study because the numerical viscosity in the code may be too dissipative and the particle size is many orders of magnitude larger than the Kolmogorov dissipation scale, $\sim d_{\rm cool}/{\rm Re} < r_{\rm jet}/10^4$. Thus the ingredients of our simulations are suitable for studing only the large-scale properties of the jet/ambient interaction.

3. SIMULATIONS

We performed several runs of a supersonic jet in a quiescent medium using different values of $\eta = n_{\rm jet}/n_{\rm amb}$ and $v_{\rm jet}$, where $n_{\rm jet}$ is the jet particle density, $n_{\rm amb}$ is the ambient particle density, $v_{\rm jet}$ is the jet velocity. The densities of protostellar jets are not well detemined, but recent observations of HH objects by Morse et al. (1992, 1993) have indicated values of $\sim 10^3$ cm^{-3}, which are significantly higher than some earlier estimates (e.g., MBB). Jet velocities have been determined from proper motions and radial velocities and range from 100–400 km s^{-1}, while typical jet radii are 0.5–4 $\times$ 10^{16} cm (MBB). For simplicity, we use a fixed value of 1000 cm^{-3} for the ambient density throughout this paper (see Bally & Lada 1983).

The parameter space of η and Mach number that we surveyed is listed in Table 1, i.e., $0.3 < \eta < 100$ and $3 < M < 110$. The Mach number, M, is defined relative to a sound speed of 12 km s^{-1}, which corresponds to an ionized plasma of 90% hydrogen and 10% helium by number at a temperature of 7000 K. Due to small timesteps in the low-density shocked gas and a slow working surface evolution, runs with, for example, $\eta = 0.1$ take several months of CPU time and thus we did not complete any runs with density ratios lower than $\eta = 0.3$. Because all flows were initially in pressure equilibrium at the jet inlet, these jets did not develop strong stationary crossing shock (X-shock) patterns.

3.1. *Effect of Jet Density on Outflow Evolution*

Figure 1 shows density contours for a $\eta = 1$, $M = 30$ jet. Figures 2*a* and 2*b* show the velocity vectors of the sph particles for light ($\eta = 0.3$) and heavy ($\eta = 10$) jets, both with $M = 30$. Since the sph particles trace the fluid these particle plots also indicate the flow density. Note that although Figures 1, 2*a*, and 2*b* show jets with different densities, the basic features are the same. At head of the jet there is a dense shell of swept-up ambient gas in the working surface (see GDPB). Behind the working surface, the jet sweeps up a dense shroud of ambient gas, which we identify with a molecular outflow. Between the shroud and the jet is a low-density cocoon containing post-shock jet gas.

TABLE 1

ENTRAINMENT EFFICIENCY

$\eta = \rho_j/\rho_a$	$M_a = v_j/c_a$	ϵ^a	$\epsilon_{BS}{}^b$
0.3.....	3	0.89	0.42
0.3.....	6	0.70	0.42
0.3.....	30	0.48	0.42
1.0.....	3	0.50	0.25
1.0.....	4.2	0.39	0.25
1.0.....	10	0.31	0.25
1.0.....	30	0.22	0.25
1.0.....	110	0.23	0.25
3.0.....	30	0.15	0.13
10.....	3	0.41	0.058
10.....	14	0.14	0.058
10.....	30	0.069	0.058
10.....	110	0.062	0.058
100.....	3	0.026	0.008
100.....	6	0.012	0.008
100.....	110	0.008	0.008

NOTES.—Sound speed c_a is 12 km s^{-1}, ambient density, ρ_a is 1000 cm^{-3}.

[a] Momentum transfer efficiency measured when jet has propogated $z = 20r_j$.

[b] Momentum transfer efficiency for a bow shock calculated from eq. (4) with $\alpha = 1$.

There are several important structural differences between the jets in Figures 1, 2*a*, and 2*b*. In Figure 2*a* the narrowing of the jet beam at the head of the jet is clearly evident. This narrowing is a result of the hot, high-pressure post-shock jet gas pushing on the sides of jet beam (see BFK; GDPB). In this narrow region the bow shock accelerates (GDPB) and thus the outflow is much narrower than the outflow closer to the source. In contrast, the heavy jet in Figure 2*b* does not develop such high pressures in the post-shock gas because of stronger cooling in the shocked gas and a lower jet shock velocity. Over the range of simulations we performed, this narrowing was found only in the light jets ($\eta = 0.3$ and 0.5).

The velocity vectors of the ambient material as shown in Figures 2*a* and 2*b* are important in understanding the

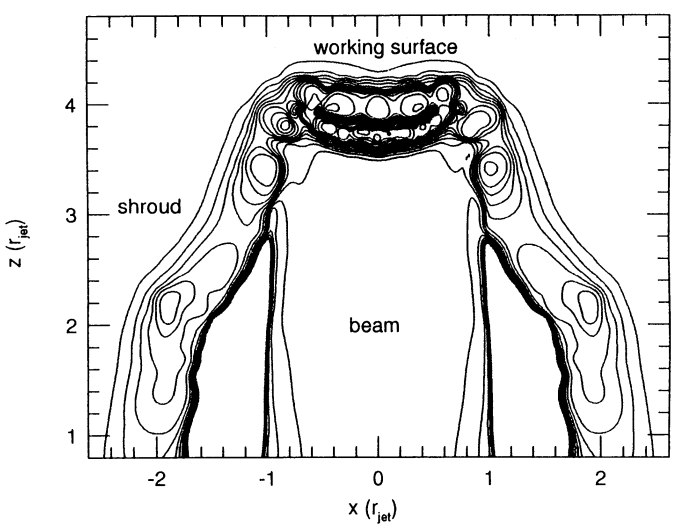

FIG. 1.—Density contours of $\eta = 1$, 350 km s^{-1} jet into a quiescent medium. The contour interval is in steps of 1.3. Note the jet beam, working surface, cocoon, and shroud as distinct features.

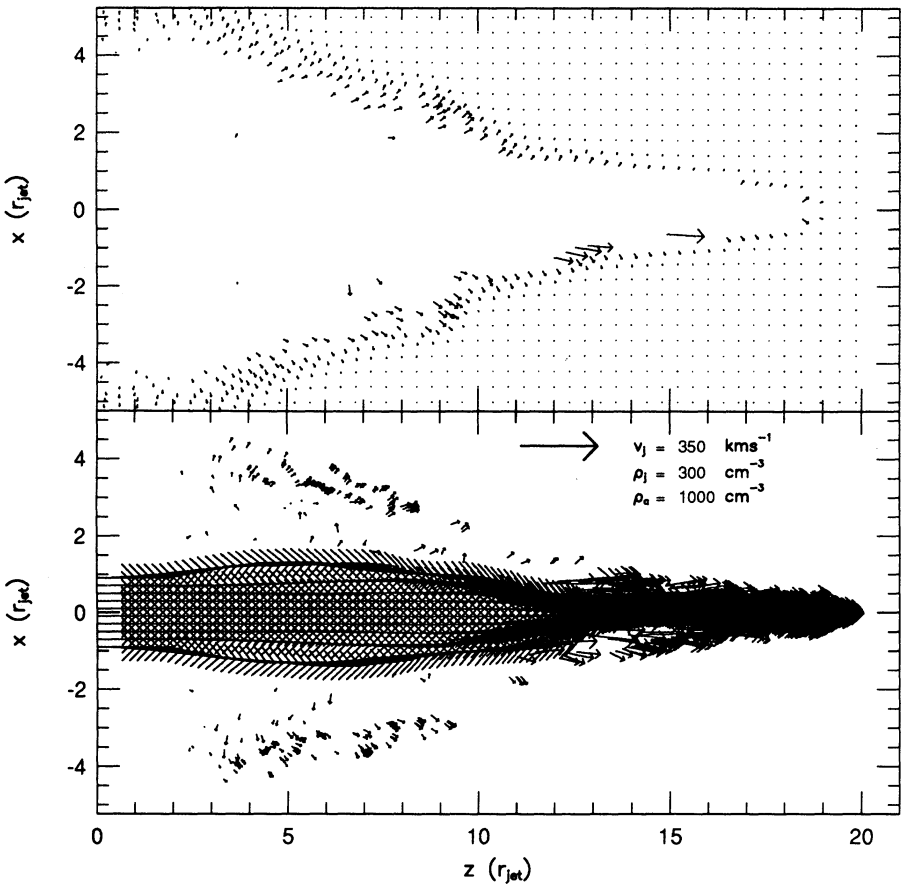

FIG. 2a

FIG. 2.—Velocity field of the sph particles within $y = \pm 0.25 r_j$ of $y = 0$. The upper pannel shows the ambient particles and the lower shows the jet particles. The length of the jet velocity vector is shown at the top right of the lower box. Jet to ambient density ratios, η of 0.3 and 10 are shown in Figures 2*a* and 2*b*, respectively. Note the different shapes of the ambient outflow in the two cases, although the general features are the same as in Fig. 1. Also note the velocity field is highest closest to the axis and mostly parallel to it.

dynamics of the interaction. At the head of the jet, close to the jet axis, the velocities are aligned with the jet, but they curve away as pressure in the shocked material accelerates the ambient material away from the jet. In the adiabatic simulations shown by De Young (1986), the ambient trajectories curve until the velocities are directed nearly normal to the jet axis. This is due to pressure in the cocoon which continually accelerates the ambient material in a direction perpendicular to the curved contact discontinuity between the cocoon and shroud. In our simulations, however, the strong cooling reduces the pressure in the cocoon and thus reduces the transverse acceleration so that the terminal velocity vectors in the shroud have directions of less than 30° away from the central axis, in good agreement with the simple assumption of the MC snowplow model. The gas in the shroud has cooled to well below 10^4 K by the time the flow in momentum driven and this can be seen to occur within one jet radius of the shock.

The effect of cooling is clearly seen in the sph ambient particle trajectories, or streaklines, which are shown in Figures 3*a* and 3*b*. The streaklines start out at small angles to the jet axis, but then curve to up to 30° away from the axis. This is due to the sideways pressure forces exerted on the shroud. The streaklines straighten out within a jet radius of the axis since pressure is no longer dynamically important and the outflow subsequently evolves in a momentum-conserving snowplow fashion.

The evolution of the cocoon can be highlighted by showing the density and pressure in planes perpendicular to the jet axis. Figures 4*a* and 4*b* show these density and pressure cuts as a function of z for $\eta = 0.3$ and 10, respectively. In both these cases the density and pressure are highest in the working surface and lowest in the cocoon surrounding the beam. Thus the undersampling of the cocoon by sph particles is acceptable given the low pressure there (for an example of the cocoon properties see Norman et al. 1982).

Thermal pressure is dynamically significant only at the working surface. Far behind the working surface the thermal pressure in the cocoon is typically of the order of $P/k = 10^6$ cm^{-3} K, while the ram pressure exerted by the shroud as it plows through the ambient material is an order of magnitude higher. Thus, as the shocked gas injected into the cocoon rapidly cools, the pressure drops and the shroud becomes momentum driven. The bulk motion of gas in the shroud continues to move away from the jet axis. Since the sound speed in the shroud is lower than the bulk velocity, there is no noticable flow back in toward the axis of the type described in the Raga & Cabrit (1993) model. However, since there are very few sph particles in the cocoon we have not accurately determined the gas motions within it.

3.2. *Effect of Mach Number on the Momentum Transfer*

In order to investigate the effect of Mach number, M, on the momentum transfer we simulated a low Mach number jet,

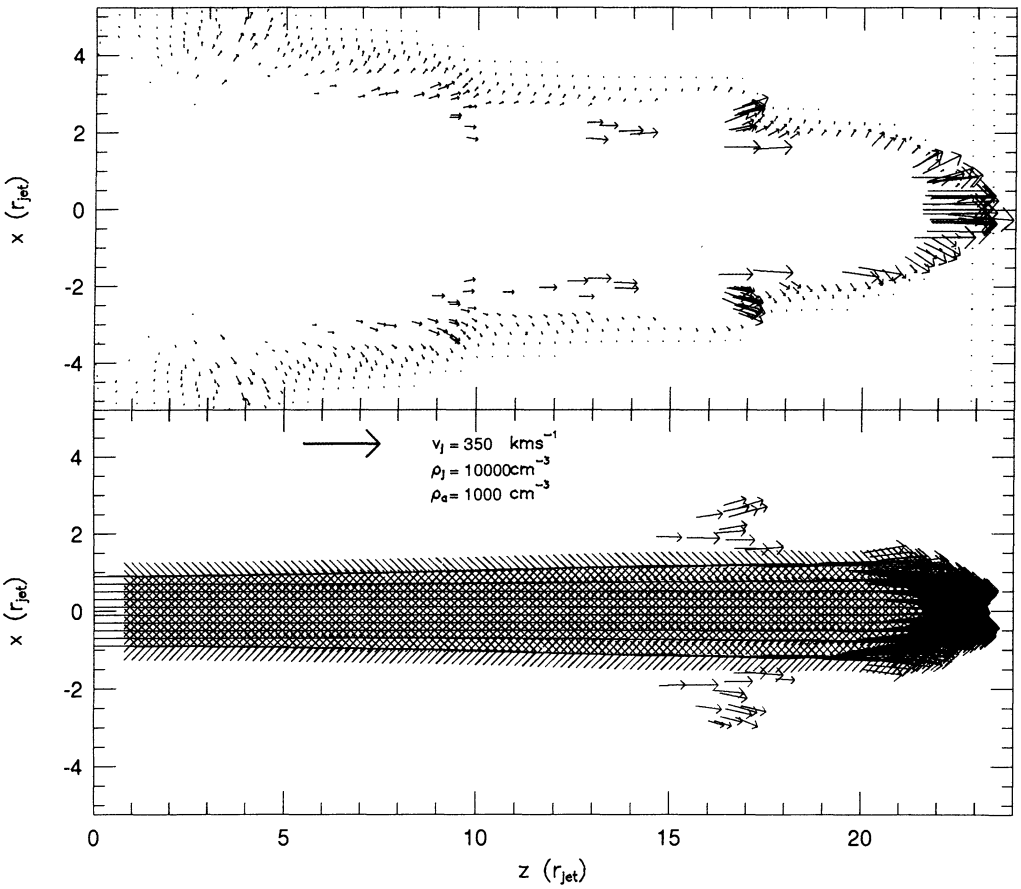

FIG. 2*b*

$M = 3$, with $\eta = 1$. Figure 5 shows the velocity vectors of the sph particles. The bow shock is significantly weaker than in the higher Mach number simulations but the shape shown is somewhat unrealistic due to edge effects at the boundary of our grid. Moreover, even though the details of the turbulence are only qualitatively correct here, it is clear that the turbulent nature of this flow is much more evident than in the higher Mach number jets (Figs. 2*a* and 2*b*). Due to a low relative velocity, the beam has been significantly disrupted by Kelvin-Helmholtz instabilities along the beam/cocoon interface (see Khan 1980). This leads to the entrainment of ambient gas into the jet flow (see top panel of Fig. 5). The entrainment is not uniform along the jet, and tends to be strongest at the center of the vorticity which is half way along the jet in Figure 5.

In Figure 6 the trajectories of the ambient sph particles in the low Mach number flow are shown. The eddies generated in the simulation are roughly the size of the jet, as limited by the code resolution. In spite of the differences in the densities and cooling, the flow pattern is similar to that of low Mach number adiabatic jets (De Young 1986). The eddies are a signature of steady state entrainment, which takes place at a high rate along the sides of this slow jet. The high velocities of the ambient material at the interface confirm that the ambient material has interacted strongly with the jet and has been accelerated. This steady state entrainment rapidly depletes the jet of its momentum and eventually results in complete disruption of the jet (see De Young 1993).

3.3. *Calculation of Bow Shock Momentum Transfer Efficiency*

The simulations above are only a small sample of the runs we performed but in this section we discuss results from the broader parameter range of Mach number, M, and density ratio, η, and apply these results to determine the general features of the momentum transfer. We use an efficiency, ϵ, that is defined as the momentum transferred to the ambient gas divided by the total momentum input. For example, when the jet has been stopped (see De Young 1993), thereby transferring all its momentum to the ambient gas, the entrainment efficiency is one. Our definition is not defined in terms of mass because of the need to define an arbitrary low-mass cutoff nor is it based on the shroud geometry as it is difficult to define a time-independent entrainment radius (see De Young 1986). Instead, we measure the efficiency at a fixed distance of propagation of the jet corresponding to the size of an outflow lobe.

The momentum transfer efficiency of a bow shock can be approximated analytically. The rate of transfer of momentum through the bow shock to the ambient medium is given by

$$\frac{dP_z}{dt} = \rho_{\rm jet} A_{\rm WS} (v_{\rm jet} - v_{\rm WS})^2 , \qquad (1)$$

where $A_{\rm WS}$ is the area of the working surface and $v_{\rm WS}$ is the velocity of the working surface. The assumption that the jet velocity, density and area are not functions of time was found to be valid for $M \geq 3$ jets over the scale of our simulations. The

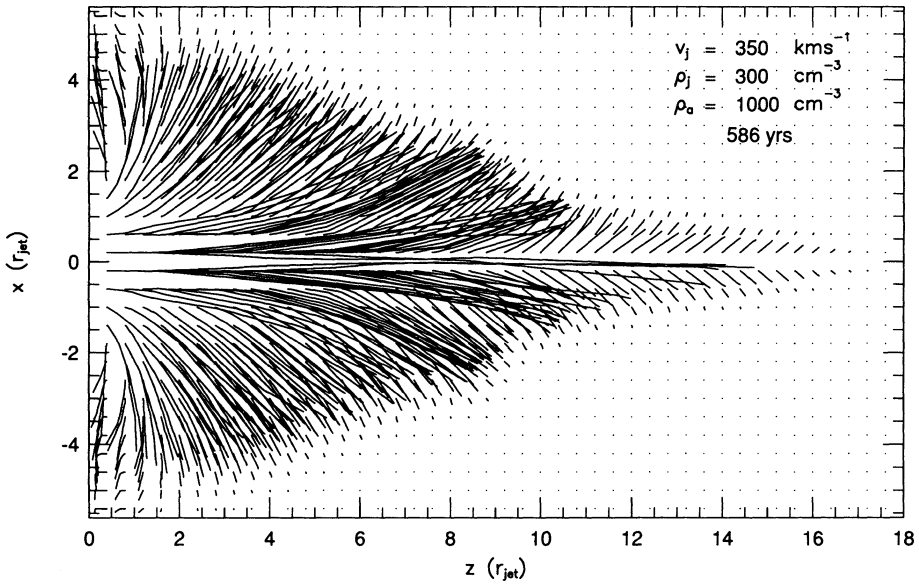

FIG. 3*a*

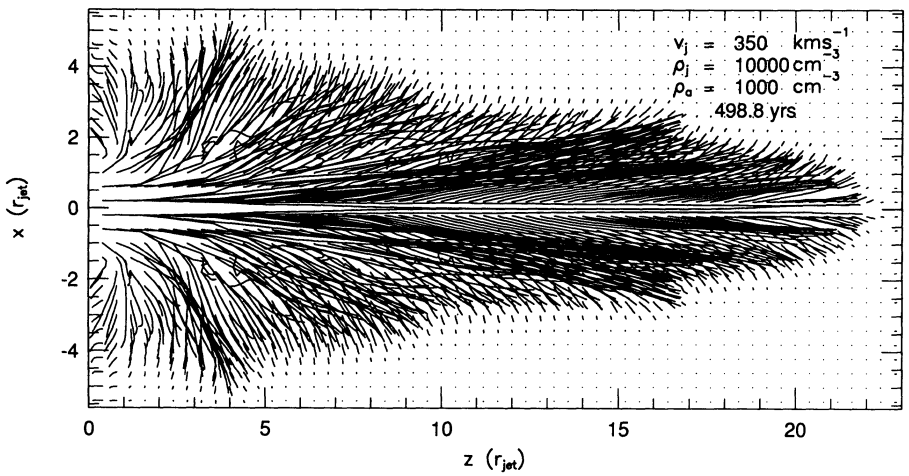

FIG. 3*b*

FIG. 3.—Streaklines of the sph particles in the ambient medium. Figures 3*a* and 3*b* show the cases of $\eta = 0.3$ and 10, respectively. Note the constant direction at large distances from the jet axis. Most of the mass in the outflow is at low velocities and only a few particles near the working surface are moving at high velocities.

total momentum input rate is $\rho_{\rm jet} v_{\rm jet}^2 A_{\rm jet}$, where $A_{\rm jet}$ is the cross sectional area of the jet inlet. Thus the ratio of momentum in the ambient medium to the total input momentum, $\epsilon_{\rm BS}$, is given by

$$\epsilon_{\rm BS} = \frac{1}{\alpha}\left(1 - \frac{v_{\rm WS}}{v_{\rm jet}}\right)^2, \qquad (2)$$

where $\alpha = A_{\rm jet}/A_{\rm WS}$ is the ratio of the jet to working surface area. Since the ram pressure at the jet shock roughly balances that at the bow shock:

$$\rho_{\rm jet} A_{\rm jet}(v_{\rm jet} - v_{\rm WS})^2 \approx \rho_a A_{\rm WS} v_{\rm WS}^2 \qquad (3)$$

and thus the entrainment efficiency of the bow shock is

$$\epsilon_{\rm BS} \approx \frac{1}{\alpha}\left[\frac{1}{1 + \sqrt{(\alpha\eta)}}\right]^2. \qquad (4)$$

To first order the jet Mach number does not affect the momentum transfer, but if the jet were freely expanding then the area factor, α would be a function of the Mach number and time.

We have used our numerical models to determine the total rate of momentum transfer, ϵ, and compared it with the calculated bow shock efficiency, $\epsilon_{\rm BS}$, assuming $\alpha = 1$. The efficiency is determined when the jet has propagated to a distance of 20 jet radii which corresponds to the size of a typical outflow lobe. The results are shown in columns (3) and (4) of Table 1 and in Figure 7. For high Mach numbers, the numerical results are in excellent agreement with equation (4), shown as a solid line in Figure 7. For low Mach numbers it is clear that the momentum transfer efficiency is significantly higher (2–3 times) than that predicted by the bow shock alone.

The increase in momentum transfer at low Mach numbers is due to a combination of two effects, an increase in the area of the working surface and turbulent entrainment along the sides

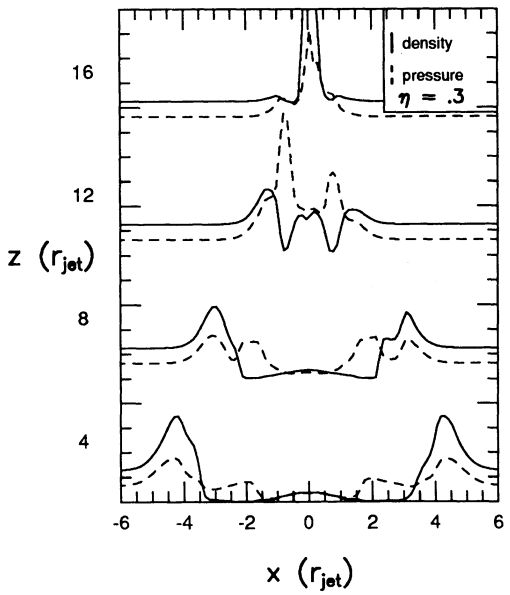

FIG. 4*a*

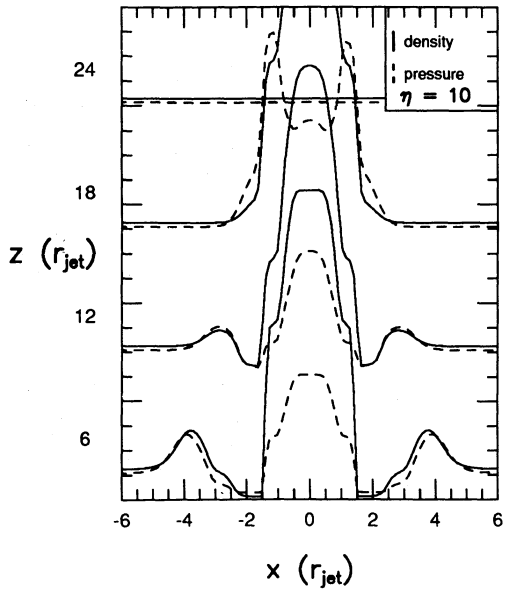

FIG. 4*b*

FIG. 4.—Density (*solid lines*) and pressure (*dashed lines*) across the flow as a function of distance from the source for a light jet ($\eta = 0.3$) and a heavy jet ($\eta = 10$) are shown in Figs. 4*a* and 4*b*, respectively. The pressure and density are very high at the working surface and are clipped in this figure as to highlight the low-level features in the outflow. The shroud is identified with a much higher density than the ambient medium. The shroud moves outwards with time sweeping up more mass and slowing down.

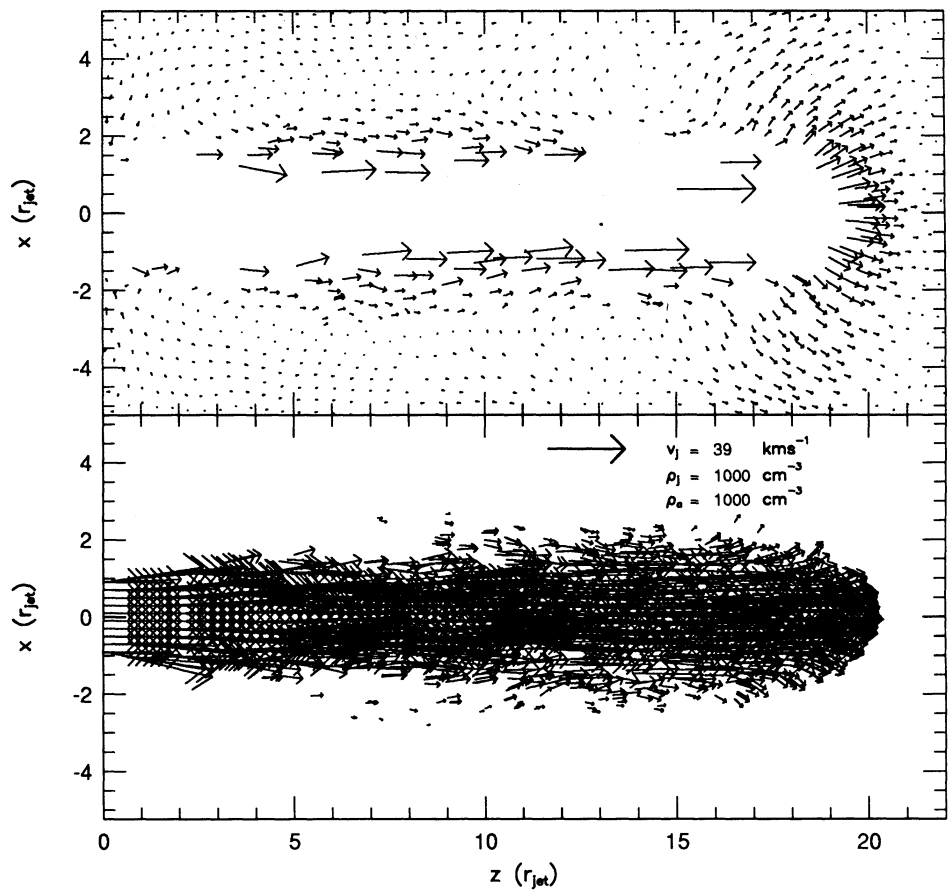

FIG. 5.—Velocity of sph particles for a jet with a low Mach number ($M = 3$). The interface between the jet and ambient medium is quite different from the higher Mach number jets shown in Fig. 2. The turbulent entrainment of ambient gas along the jet beam is clearly evident in the upper panel.

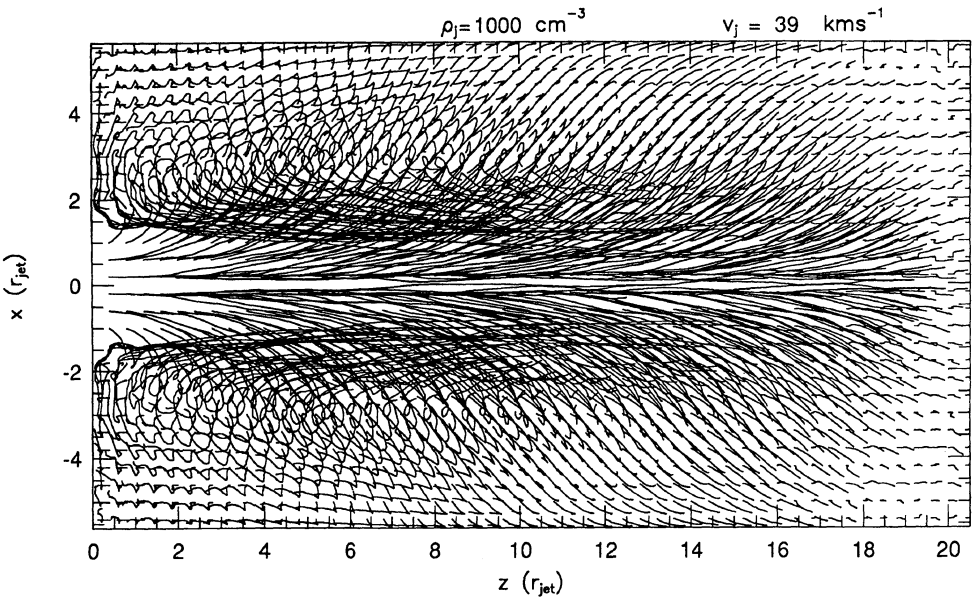

FIG. 6.—Tracing of the ambient sph particles for a jet with a low Mach number, (M = 3). The turbulent eddies are similar to the flow shown in De Young (1986). The turbulent steady state entrainment along the beam is as significant as the prompt momentum transfer by the bow shock.

of the jet. A lower Mach number jet expands into the cocoon at a wider angle due to its lower forward velocity relative to the sound speed. The expansion of the jet can be reversed by recollimation (Norman et al. 1982) by the ambient medium. However, it is through this close contact with the ambient medium that turbulent entrainment takes place.

The importance of steady state entrainment can be studied by examining the deceleration of the jet (De Young 1986). This can be done by plotting the velocity along the jet axis as is shown in Figures 8*a* and 8*b* for low (M = 3) and high Mach number (M = 30) jets, respectively. The velocity has been determined by averaging *over* the particles within the volume of the jet. The histrogram shows the jet particles and the heavy solid line shows the ambient particles. Note that the low Mach number, M = 3, jet is strongly decelerated at $z = 3r_j$ which corresponds to the location of the first crossing shock. The jet starts transferring momentum to the ambient medium here, as shown by the high velocities in the ambient medium. On the other hand, the jet gas in the high Mach number jet is decelerated only at the jets working surface and there is essentially no entrained material in the jet before it reaches this point. This is the essential difference between the two processes described by De Young (1986). In the prompt process momentum is transferred entirely at a working surface and in the steady state process momentum can be transferred anywhere along the length of the jet. We therefore attribute the increase in ϵ at low Mach numbers to the steady state process.

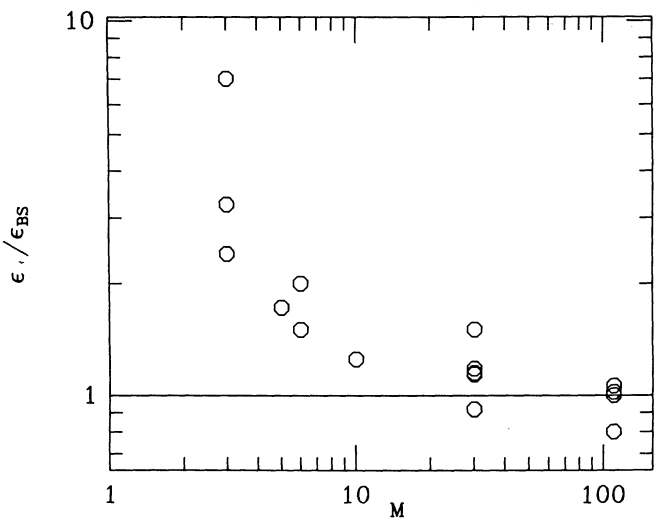

FIG. 7.—Momentum transfer efficiency measured from the simulations divided by the prompt efficiency calculated from eq. (4). The data are given in Table 1. Note the strong departure from the prompt efficiency for low Mach number flows (i.e., $\epsilon > \epsilon_{BS}$). This departure is attributed to turbulent entrainment along the beam.

The steady state process is dominant in most examples of supersonic lab jets in which the jet disruption is readily observed (De Young 1993). However, protostellar jets interacting with cold, dense, molecular clouds are highly supersonic and therefore transfer their momentum mainly at the working surfaces. If protostellar jets were decelerated along their length then one would not expect high-velocity shocks and HH objects to be found at the ends of the outflow lobes (MBB; Chernin & Masson 1991).

4. COMPARISON WITH MODELS

The above results exemplify the interaction between a supersonic jet and dense ambient gas under the conditions relevant to protostellar molecular outflows. At high Mach numbers, the prompt process dominates. Under these conditions, the bow shock is strongly radiative and the outflow is driven initially by thermal pressure, but later evolves in a momentum-conserving fashion, because of the strong cooling. In higher Mach number flows the working surface shocks are strong and push the cocoon away from the jet, separating the ambient material from the jet, and inhibiting turbulent entrainment. With low Mach number jets there is less pressure ($T \sim v_s^2$) available to accelerate the shroud, and furthermore the ambient gas is better able to react to the presence of the jet. The M = 3 simu-

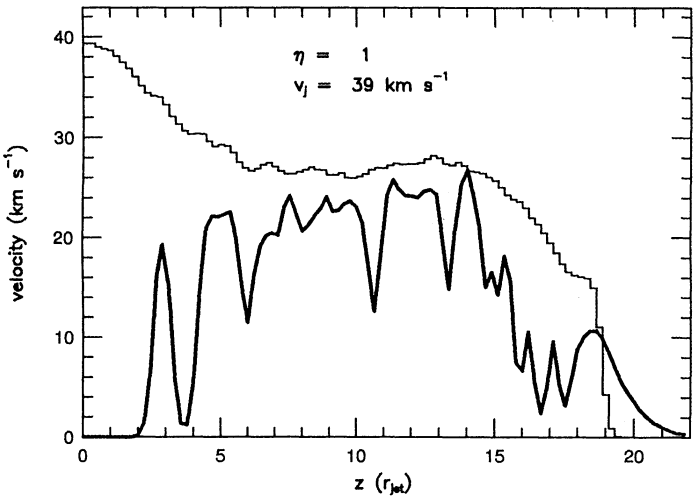

FIG. 8a

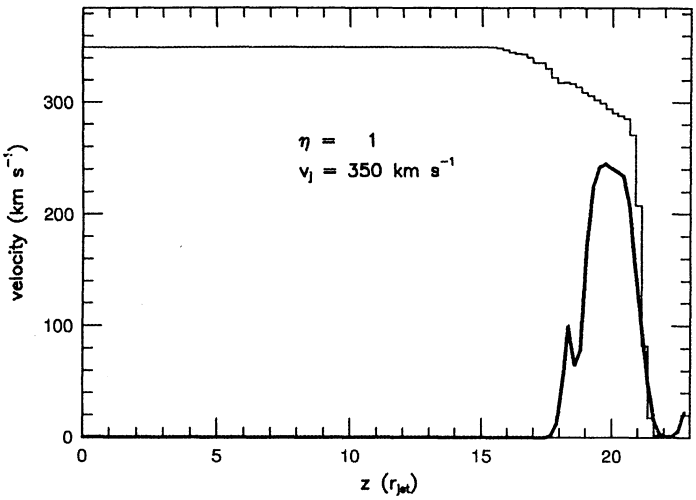

FIG. 8b

FIG. 8.—Mass-weighted average velocity along the flow axis for a $M = 3$ jet (*a*) and a $M = 30$ jet (*b*). The histogram corresponds to the jet particles and the heavy solid line corresponds to the ambient particles. Note the strong initial deceleration of the $M = 3$ jet which corresponds to the acceleration of ambient gas. The sharp accelerations and decelerations of the ambient gas close to the working surface in the high Mach number jet are similar to features seen in high-resolution position-velocity diagrams of outflows (MC).

lation (Figs. 5 and 6) demonstrates the nature of the flow under favorable conditions for the steady-state process (see De Young 1986). The ambient particles in the path of the beam are not pushed far from the axis of the jet, leaving only a thin cocoon, which is not sufficient to prevent backflow and subsequent turbulent mixing between the ambient and jet particles.

Since Mach numbers of protostellar jets are 10–40 (see MBB), we conclude that under these conditions the steady state entrainment is not an important momentum transfer process, and the jets primarily transfer momentum to the ambient medium at the working surface. Thus the turbulent mixing models of Lizano et al. (1988) and Stahler (1993) which describe conditions closer to those found in our low Mach number simulations are not appropriate for molecular outflows. Also these models cannot easily account for HH objects at large distances from the star, since they predict a steady decrease in velocity along the flow.

The RC model of the molecular outflow as a turbulent wake that results from the infall of the swept-up gas is not confirmed by our simulations which show that the shroud has significantly cooled by the time the jet has propagated to the end of the outflow lobe. Based on our simulations, we estimate the timescale for the swept-up gas to refill the cavity as of the order of the maximum size of the shroud divided by the local sound speed, or $\approx(10^{17}$ cm)/(1 km s^{-1}) $= 4 \times 10^4$ yr ($\approx$80 jet crossing times), so that only the longest term evolution should be affected by refilling. However, if there is a component of the shroud with a higher Alfvén speed or sound speed then the cavity may refill on a shorter timescale. The MC model agrees well with the simulations presented here and provides a good approximation to the interaction between a jet and a molecular cloud short timescales. However, it does not treat long term evolution in any detail, and something like the RC and RCCRT models may be more applicable at late times.

5. COMPARISON WITH OBSERVATIONS

Over the last few years high-resolution millimeter and submillimeter observations of molecular outflows have shown that the structure of the high-velocity gas ($v > 30$ km s^{-1}) is significantly different from that of the low-velocity gas (e.g., Masson, Mundy, & Keene 1990; Bachiller, Martin-Pintado, & Planesas 1990; Bachiller et al. 1991; Chernin & Masson 1992; Richer, Hills, & Padman 1992). The higher velocity material in the outflow gas is more collimated, spatially confined, concentrated along the outflow axis, and shows greater accelerations and decelerations than the low-velocity gas. These features all suggest that the outflow is jet driven, and in particular, we show below that the recently discovered extremely high-velocity (EHV) CO features (see Lizano et al. 1988, Masson et al. 1990; Bachiller et al. 1990) can be accounted for by bow shocks.

In Figure 9 we show the mass distribution of the particles as a function of velocity for a $\eta = 1$ jet. The velocity has been determined by averaging the particles over the line of sight in a cylinder twice as wide as the jet. The histogram shows the jet particles, and the solid line shows the ambient particles. In

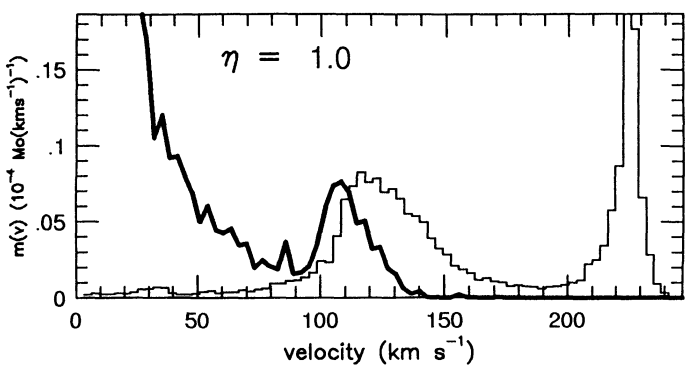

FIG. 9.—Mass-velocity profiles along a 55° line of sight of an $\eta = 1$ jet. The histogram shows the jet particles, and the solid line shows the ambient particles. Note the two components in the jet distribution corresponding to the pre- and post-shock gas. We suggest the EHV CO features correspond to molecules formed in the post-shock gas. The bump at 100–120 km s^{-1} has similar dynamical properties to the EHV feature observed in HH 7–11 (Masson et al. 1990).

Figure 9 note that the low-velocity end of the distribution shows a decrease in mass with velocity which is a characteristic of a swept-up flow (see Masson & Chernin 1992). However, we concentrate our discussion of the velocity distribution on the high-velocity components, since the timescale of our simulation is only a few hundred years while the low-velocity gas in real outflows is accumulated over tens to hundreds of thousands of years and thus is not accurately represented here.

In the $\eta = 1$ jet, the post-shock jet gas forms an EHV feature at 120 km s^{-1} with a total mass of 10^{-3} $M_\odot$ and velocity FWHM of 20 km s^{-1}. This EHV gas is located just behind the apex of the bow shock but the gas slows down rapidly and cools in the snowplow. These features are comparable with the observations of HH 7–11 (Masson et al. 1990) which show $\sim 10^{-3}$ $M_\odot$ at 100–120 km s^{-1}. We suggest the EHV features are the result of the small spatial and velocity ranges in the shocked gas. An alternative model of the EHV CO arising from quiescent gas inside molecular "bullets" (Bachiller et al. 1990) or molecular winds (Koo 1990) cannot easily explain the large line widths (10–30 km s^{-1}) since the gas in the EHV gas has temperatures of only 30–100 K (Masson et al. 1990; Chernin & Masson 1992). In contrast to a molecular wind or bullet models, the EHV line width in the shocked gas in the jet-driven model is determined by the pressure (probably magnetic) in the compressed, post-shock gas and not by the temperature of the gas.

The EHV CO is observed at velocities for which molecules would be dissociated in (nonmagnetic) shocks (see Hollenbach 1980). However, Neufeld & Dalgarno (1989a, b) and Hollenbach & McKee (1989) have suggested that molecules can reform on grains after the passage of a dissociative shock. A simple constraint on this scenario is that the post-shock column densities need to be greater than 10^{20} cm^{-2} before molecules form, requiring a time of

$$320\left(\frac{n}{1000\ \mathrm{cm}^{-3}}\right)^{-1}\left(\frac{v_{\mathrm{shock}}}{10^7\ \mathrm{km\ s}^{-1}}\right)^{-1}\ \mathrm{yr}\ .$$

Since the transit times of jets across an outflow lobe are only a few hundred years, EHV CO would only be reformed in dense gas that must have at least 10^3 cm^{-3}. This pre-shock, dense molecular gas may be initially in the jet (ambient medium) and be dissociated by the jet (bow shock). In the case of reformation of dense ambient molecular gas, the jets must be quite dense since the bow shock velocity must be at least 60–150 km s^{-1} to account for the observations. The above constraint calculation is very crude, since our simulations do not consider the behavior of the gas as it becomes molecular, and the shock chemistry calculations are based on planar one-dimensional shocks, but we suggest that our jet model gives a plausible explanation for the observed EHV CO features (see Chernin & Masson 1992). In fact, molecule formation will probably occur at lower column densities since in three dimensions the UV radiation field in the recombining gas is more dilute than in a one-dimensional shock. Moreover, magnetic fields can remove some of the shock energy and may account for the finite width of the EHV features of 10 km s^{-1} as this is close to the Alfvén speed in the post-shock gas.

A second observational characteristic of outflows is the wide range of velocities sometimes seen in a small region near the EHV features, indicating sharp increases and decreases in the velocity. MC identified this material with a bow shock. Due to computational limitations there are not enough sph particles in the working surface region to make a position—velocity diagram that can be accurately compared with observations. Instead we measured the average velocity of the particles in planes perpendicular to the flow axis. Figure 8*b* showed an example of this in which the accelerations and decelerations at the working surface are clearly evident.

6. SUMMARY

We performed numerical simulations of jets over the range of conditions expected in the protostellar environment. The strongly cooling shocks do not produce high-pressure lobes around the jet as in the case of extragalactic jets and thus protostellar outflows evolve in a momentum conserving snowplow fashion. This result confirms the basic scheme of the MC model. That model well represents the youngest outflows ($t < 2 \times 10^4$ yr), however our simulations do not cover the evolution of older outflows which may be up to 2×10^5 yr old (Parker, Padman & Scott 1991; Parker et al. 1989). The Raga & Cabrit (1993) model may better represent the later evolution of the swept-up gas if the swept-up gas refills the cavity at a significant rate.

Entrainment of ambient gas along the jet beam is only important in low Mach number flows ($M < 6$) while typical protostellar jets have $10 < M < 40$. Momentum transferred to ambient gas is therefore mostly prompt, i.e., through the leading bow shock and a simple analytic calculation of the efficiency of momentum transfer agrees with our numerical results over a wide parameter space.

In principle, our entrainment model can be used to estimate the poorly known parameters of the outflows such as the ages and jet densities. This paper is only a first step in numerical modeling of protostellar outflows. The effects of changes in the jet direction, jet intermittency (see MC), and density gradients on our model have yet to be determined. Spatial and temporal variations in the jet and ambient medium undoubtedly play a role. For example the effects of intermittent jets and atmospheric density gradients have been studied under various conditions by RC, RCCRT, Gouveia Dal Pino & Benz (1994), Gouveia Dal Pino, Birkinshaw, & Benz (1994), and MC. Future modeling of these effects and simulations with much greater ages will be important in comparing theory with higher resolution observations such as those of Carlstrom (1994) and Padman & Richer (1993).

We would like to thank Mark Birkinshaw for helpful suggestions.

REFERENCES

Bachiller, R., Cernincharo, J., Martin-Pintado, J., Tafalla, M., & Lazareff, B. 1990, A&A, 231, 174
Bachiller, R., Martin-Pintado, J., & Planesas, P. 1991, A&A, 251, 639
Bally, J., & Lada, C. J. 1983, ApJ, 265, 824
Benz, W. 1990, in Numerical Modeling of Stellar Pulsations: Problems and Prospects, ed. J. R. Bulcher (Dordrecht: Kluwer), 269
———. 1991, in Late Stages of Stellar Evolution and Computational Methods in Astrophysical Hydrodynamics, ed. C. de Loore (Berlin: Springer), 259
Blondin, J. M., Fryxell, B. A., & Königl, A. 1990, ApJ, 360, 370 (BFK)
Blondin, J. M., Königl, A., & Fryxell, B. A. 1989, ApJ, 337, L37
Cantó, J., & Raga, A. 1990, ApJ, 372, 646
Carlstrom, J. E. 1994, in preparation
Chernin, L., & Masson, C. R. 1991, ApJ, 383, L93
———. 1992, ApJ, 396, L35
De Young, D. S. 1986, ApJ, 307, 62
———. 1993, ApJ, 420, 95

Dyson, J. E., Cantó, J., & Rodriguez, L. F. 1988, in Mass Outflows from Stars and Galactic Nuclei, ed. L. Bianchi & R. Gilmozzi (Dordrecht: Kluwer), 299
Edwards, S., & Snell, R. L. 1983, ApJ, 270, 605
Fukui, J. 1989, in Low-Mass Star Formation and Pre–Main-Sequence Objects, ed. Bo Reipurth (Garching: ESO), 95
Glassgold, A. E., Mamon, G. A., & Huggins, P. J. 1989, ApJ, 336, L29
———. 1991, ApJ, 373, 254
Gouveia Dal Pino, E. M., & Benz, W. 1993, ApJ, 410, 686 (GDPB)
———. 1994, ApJ, submitted
Gouveia Dal Pino, E. M., & Birkinshaw, M., & Benz, W. 1994, in preparation
Hartigan, P., Raymond, J., & Hartmann, L. 1987, ApJ, 316, 323
Hollenbach, D. J., & McKee, C. F. 1979, ApJS, 41, 555
———. 1989, ApJ, 342, 306
Katz, J. 1989, Ph.D. thesis, Princeton Univ.
Khan, F. 1980, A&A, 83, 303
Koo, B-C. 1990, ApJ, 361, 145
Lada, C. J. 1985, ARA&A, 23, 267
Liseau, R., Sandell, G., & Knee, L. B. G. 1988, A&A, 192, 153
Lizano, S., et al. 1988, ApJ, 328, 763
Masson, C. R., & Chernin, L. M. 1992, ApJ, 387, L47
———. 1993, ApJ, 414, 230 (MC)
Masson, C. R., Mundy, L. G., & Keene, J. B. 1990, ApJ, 357, L25
McKee, C. F., & Hollenbach, D. J. 1987, ApJ, 322, 275
Morse, J. A., Hartigan, P., Cecil, G., Raymond, J. C., & Heathcote, S. 1992, ApJ, 399, 231
Morse, J. A., Heathcote, S., Hartigan, P., & Cecil, G. 1993, AJ, 106, 1139
Mundt, R., Brugel, E. W., & Bührke, E. 1987, ApJ, 319, 275 (MBB)
Neufeld, D., & Dalgarno, A. 1989a, ApJ, 340, 869
———. 1989b, ApJ, 344, 251
Norman, M. L., Smarr, L., Winkler, K-H., & Smith, M. D. 1982, A&A, 113, 285
Padman, R., & Richer, J. 1993, in Kinematics and Dynamics of Diffuse Astrophysical Media, ed. J. Dyson (Dordrecht: Kluwer), in press
Parker, N. D., Padman, R., & Scott, P. F. 1991, MNRAS, 252, 442
Parker, N. D., Padman, R., Scott, P. F., & Hills, R. F. 1989, MNRAS, 234, 67P
Raga, A. C. 1988, ApJ, 335, 820
Raga, A. C., & Cabrit, S. 1993, A&A, 278, 267 (RC)
Raga, A. C., Canto, J., Calvet, N., Rodriguez, L. F., & Torrelles, J. 1993, A&A, 276, 539 (RCCRT)
Ray, T. P., Poetzel, R., Solf, J., & Mundt, R. 1990, ApJ, 357, L45
Reipurth, B. 1991, in the Physics of Star Formation and Early Stellar Evolution, ed. C. J. Lada & N. D. Kylafis (Dordrecht: Kluwer), 497
Richer, J. S., Hills, R. E., & Padman, R. 1992, MNRAS, 254, 525
Shu, F. H., Lizano, S., Ruden, S. P., & Najita, J. 1989, ApJ, 328, L19
Shu, F. H., Ruden, S. P., Lada, C. J., & Lizano, S. 1991, ApJ, 370, L31
Stahler, S. 1993, in Astrophysical Jets, ed. M. Livio, C. O'Dea, & D. Burgarella (Cambridge: Cambridge Univ. Press), in press
Tenorio-Tagle, G., Canto, J., & Rózyczka, M. 1988, A&A, 202, 256
Van Dyke, M. 1982, An Album of Fluid Motion (Stanford: Parabolic Press)